AIP | Physics of Fluids

Numerical studies of vortex-induced extinction/reignition relevant to the near-field of high-Reynolds number jets

Rishikesh Venugopal and John Abraham

Citation: Phys. Fluids 21, 055106 (2009); doi: 10.1063/1.3139308
View online: http://dx.doi.org/10.1063/1.3139308
View Table of Contents: http://pof.aip.org/resource/1/PHFLE6/v21/i5
Published by the American Institute of Physics.

Numerical studies of vortex-induced extinction/reignition relevant to the near-field of high-Reynolds number jets

Rishikesh Venugopal and John Abraham[a)]
School of Mechanical Engineering, Purdue University, West Lafayette, Indiana 47907, USA

(Received 25 July 2008; accepted 2 April 2009; published online 27 May 2009)

This work is motivated by the need to understand physical mechanisms governing near-field phenomena, such as flame lift-off, in high-Reynolds number jet flames. Numerical studies of vortex-induced flame extinction/reignition are performed for conditions representative of the near field of high-Reynolds number (~100 000) jets under high pressure and temperature conditions. The governing equations for compressible, viscous, and reacting flows are solved along with a single-step irreversible chemical kinetic model for gaseous *n*-heptane oxidation. Extinction/reignition phenomena, influenced by unsteady and curvature effects, are observed. Unsteady flamelet/progress variable models are shown to accurately describe the flame response during extinction/reignition observed in the flame-vortex studies. Furthermore, while unsteady effects on extinction/reignition are found to diminish with weaker vortices and relatively strong flames, curvature effects are found to increase with relatively thicker flames. The observed flame-vortex interaction regimes are summarized on an outcome diagram, which is useful to understand the nature of localized flame dynamics in the near field of jet flames. © *2009 American Institute of Physics*. [DOI: 10.1063/1.3139308]

I. INTRODUCTION

Recent experiments[1,2] in diesel jet flames have shown that flame lift-off has a significant influence on pollutant formation through fuel/air premixing in the jet near field. Hence, understanding lift-off, and the development of predictive computational tools for diesel jet flames are important. Recent attempts in literature[3] to numerically predict diesel flame lift-off with conventional Reynolds-averaged Navier–Stokes (RANS)-based modeling approaches, such as steady diffusion flamelets[4] and perfectly stirred reactors[5] have met with only limited success. RANS models are also inadequate in reproducing the mixing and entrainment characteristics in the jet-near-field region where lift-off occurs.[6] In addition, jet near-field phenomena contributing to lift-off could result from a combination of physical processes, such as autoignition,[7] partially premixed flame propagation,[8,9] and local extinction/reignition,[8] and a detailed understanding of these phenomena through fundamental studies is required.

In the present work, we focus attention on the simulation of local flame extinction/reignition through flame-vortex interaction studies. We consider an initially flat diffusion flame that interacts with a counter-rotating vortex pair and undergoes extinction/reignition. We note that this is one of the possible scenarios for the local flame dynamics at the lift-off height of a jet flame. Other canonical configurations, such as triple-flame-vortex interactions, which are relevant to understanding lift-off, have been studied in prior works.[10] The pressure and temperature chosen are representative of diesel engine combustion chambers. The range of length and velocity scales of the simulated vortices, and the scalar dissipation rates characterizing the diffusion layers are relevant to the near field of high-Reynolds number (~100 000) jets. In spite of its configurational simplicity, the flame-vortex setup is useful to study detailed effects due to unsteadiness and curvature, and to assess the accuracy of turbulent combustion models, such as flamelet models. Here, we evaluate the capability of steady-flamelet and unsteady flamelet/progress variable models to predict flame extinction/reignition. Now, we will briefly review prior works on flame-vortex interactions relevant to nonpremixed flame extinction/reignition.

In steady diffusion flames, it is well known that extinction can be characterized by the steady extinction limit χ_e, which is essentially the scalar dissipation rate beyond which a steadily strained flame cannot be sustained.[9,11] However, recent studies on vortex-perturbed flames[12–15] have shown that unsteady extinction limits could be higher than steady values. For instance, in the recent studies of Venugopal and Abraham[15] under typical diesel engine conditions, unsteady limits about ten times higher than χ_e were observed due to characteristic chemical-to-vortex time scale ratios much greater than unity. In other words, if the characteristic response time scale of the flame is slower than the imposed flow time scale, then large deviations from steady behavior may be observed due to delayed flame response. Moreover, prior studies on flame-vortex interactions[14,15] suggest that unsteady extinction limits are flow dependent, and increase with increase in the vortex velocity scale. In the present work, we will corroborate some of these findings on unsteady flames, and discuss an extinction criterion that is applicable in unsteady flow fields.

In addition to unsteady effects on extinction, reignition has received attention through experiments on vortex-perturbed flames,[16,17] and numerical studies in reacting iso-

[a)]Author to whom correspondence should be addressed. Electronic mail: jabraham@ecn.purdue.edu.

tropic turbulence[18] and flame-vortex interactions.[15,19,20] The direct-numerical-simulation (DNS) study of Sripakagorn *et al.*[18] in reacting isotropic turbulence employing a single-step kinetic model revealed three modes of reignition: an independent-flamelet scenario, where the extinguished flamelets reignite through autoignition, an edge-flame propagation scenario, where reignition occurs through propagation of edge flames, which are extremities of diffusion flame holes,[21] and an engulfment scenario, where turbulent convection of hot products from neighboring burning regions leads to reignition. Sripakagorn *et al.*[18] reported that when the excursions of χ over χ_e are relatively large, reignition is likely to occur through edge-flame propagation and engulfment scenarios. This trend was confirmed in our recent flame-vortex interaction studies with both single-step[15] and multi-step *n*-heptane chemistries,[20] where reignition was found to occur through edge-flame interactions governed by vortex-induced curvature. In particular, it was shown that while the extinction phase is dominated by unsteady effects, the reignition phase is controlled by both unsteady and curvature effects. Essentially, due to relatively high scalar dissipation rates ($>\chi_e$) during unsteady extinction, the gradients in the flame-normal direction are much higher than those along the lateral (i.e., along the flame surface) direction, leading to minimal curvature effects. However, the presence of the rolled-up edge flames bordering the quenched regions during reignition leads to substantial gradients in the lateral direction, so that curvature effects become important in addition to unsteady effects. Furthermore, recent experimental and numerical studies of Amantini *et al.*[22,23] employing a double-vortex-flame configuration confirm the importance of edge-flame propagation scenarios in unsteady extinguishing/reigniting flames. In the present work, we will investigate how trends in unsteady extinction/reignition phenomena change in the near field of the jet, and present a modeling framework to account for the extinction/reignition phenomena observed in the flame-vortex studies.

Based on the review of prior works, it is evident that unsteady extinction/reignition has received prior attention, but not in the context of high-Re jets under diesel engine conditions. In particular, it is not known how extinction/reignition scenarios depend on localized effects due to unsteadiness and curvature in the near field of a high-Re jet. In addition, commonly employed modeling approaches, such as steady-flamelet models,[9] need assessment for the prediction of unsteady extinction/reignition. Hence, we specifically address the following two questions: (a) How does unsteadiness and curvature affect local flame extinction/reignition in the near-field of high-Re jets? (b) What modeling approaches are applicable to predict unsteady extinction/reignition in the jet near-field? From an application viewpoint, answers to these questions can aid the development of improved numerical models that can lead to accurate predictions of jet near-field phenomena, such as flame lift-off, and their effects on pollutants. From a fundamental viewpoint, useful physical insights can be gained into flow-chemistry interactions involved in less-understood combustion phenomena, such as unsteady extinction/reignition in nonpremixed flames.

In Sec. II, the numerical formulation, and computational

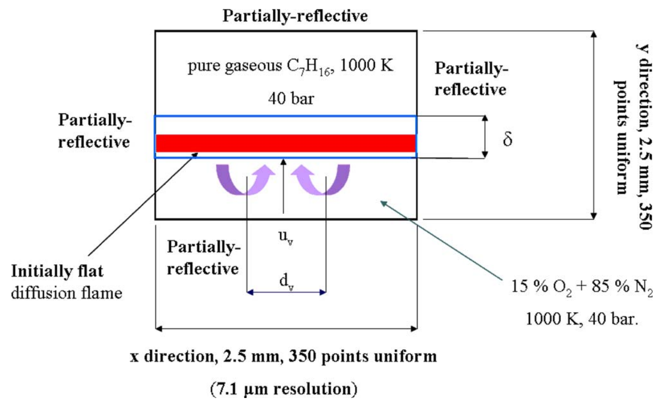

FIG. 1. (Color online) Computational setup for the flame-vortex studies.

setup and conditions employed for the flame-vortex interaction studies are discussed. Results and discussion follow in Sec. III. This paper closes with summary and conclusions in Sec. IV.

II. NUMERICAL FORMULATION

The flame-vortex studies are performed with the two-dimensional (2D) version of the flow, large-eddy, and direct simulation (FLEDS) code,[15,20] which has been developed in-house and used in several prior studies of nonreacting[24] and reacting shear layers,[15,20,25] and large eddy simulation (LES) of nonreacting jets.[26] A detailed discussion of the numerical formulation, including the governing equations, implementation of numerical schemes and boundary conditions may be found in a recent publication.[26] FLEDS solves the full governing equations for compressible, viscous, and reacting flows. The sixth-order compact finite-difference scheme of Lele[27] is implemented for spatial discretization, while time integration is performed with a compact-storage fourth-order Runge–Kutta scheme.[28] For the flame-vortex simulations, partially reflective boundary conditions are implemented on all the boundaries using the Navier–Stokes characteristic boundary conditions method of Poinsot and Lele,[29] extended to account for the presence of multicomponent gaseous mixtures.[26]

Figure 1 shows the computational setup. A 2D computational domain with a uniform resolution of about 7 μm is employed. In the present work, the initial vortex length scales (d_v in Fig. 4) simulated lie in the range of 100–600 μm, and the initial diffusion layer thicknesses (δ) lie in the range of 150–500 μm. Hence, the chosen resolution resolves the relevant length scales of the flame-vortex interaction by at least 15 cells, which is consistent with the typical choice of about ten cells to resolve the relevant length scales in DNS studies.[8] Note that for the larger vortices ($d_v > 200$ μm) and thicker diffusion layers ($\delta > 200$ μm) employed, larger domains (5×5 mm^2) with the same resolution, i.e., 7 μm, are used. In addition, the domain sizes chosen are at least eight times larger than the simulated vortices in either direction to minimize boundary effects. Our recent studies[20] show that the chosen resolution is sufficient to adequately describe the physical mechanisms governing extinction/reignition for the conditions employed here.

An initially flat diffusion flame is established between pure n-heptane at 1000 K one side, and diluted air (15% O_2+85% N_2 molar composition) on the other side. The simulated pressure is 40 bars. These conditions are representative of diesel engine combustion chambers, with the exception of the fuel-side temperature, which is higher than those typically employed in diesel engines ($\sim$400 K). Higher fuel-side temperatures (=1000 K) will result in stronger flames, and higher limiting scalar dissipation rates for extinction/reignition, as well as kinetic effects, such as transition from two-stage to single-stage autoignition.[30] In our work, which employs a single-step kinetic model, the choice of a higher fuel temperature reflects in a shorter chemical time scale, which, in turn, affects nondimensional numbers, such as the Damkohler number, and length and velocity scale ratios between the vortex and the flame. Similarly, the choice of the higher pressure (=40 bars) to emulate diesel engine conditions primarily affects the Damkohler number through the chemical time scale. As discussed in our recent studies under diesel conditions,[20] the ideal gas equation of state is adequate even at these high pressures (=40 bars) due to the predominant presence of diluents such as N_2 in the flame zone. The choice of simple chemistry precludes the resolution of kinetic effects due to the higher temperatures and pressures. This is, however, consistent with our primary motivation of studying flame-vortex interaction regimes under diesel engine conditions.

It is evident that the use of a 2D formulation ignores three-dimensional (3D) effects, such as vortex stretching, on the flame dynamics. The 2D assumption is typical in flame-vortex simulations,[31] including recent 2D flame-vortex studies,[14,15,23] which have provided useful insights into unsteady and curvature effects on nonpremixed flame structure. Although 3D effects on vortex-perturbed flames have received limited attention in literature, the analytical work of Karagozian and Marble[31] showed that the augmentation of the reactant consumption rate by the vortex is independent of vortex stretching effects, which primarily manifest in the distribution of the combustion products in the vortex-perturbed flame. Nevertheless, we will highlight the implications of the 2D assumption on the unsteady extinction/reignition scenarios observed in this work.

To simulate the vortex perturbation, an Oseen–Hammel[32] counter-rotating vortex pair is superimposed on the initial flow field. Details of the vortex implementation may be found in Ref. 19. We employ a single-step kinetic model[15] for n-heptane oxidation, i.e.,

$$F + \nu_O O_2 \rightarrow \nu_P P, \tag{1}$$

where F represents the fuel, P represents the primary products of combustion, and ν denotes the stoichiometric coefficient. If F represents n-heptane, C_7H_{16}, which is a commonly employed surrogate for practical fuels like diesel, then $\nu_O=11$ and $\nu_P P=7CO_2+8H_2O$. The single-step model results in a unique chemical time scale τ_c, which may be estimated as[33]

$$\tau_c = \left(\frac{\dot{w}_P \mathrm{MW}_{\mathrm{mix}}}{\rho}\right)^{-1} = \left(\frac{\nu_P A T^b [F]^m [O_2]^n \exp\left(-\dfrac{E_a}{R_u T}\right) \mathrm{MW}_{\mathrm{mix}}}{\rho}\right)^{-1}, \tag{2}$$

where $\dot{w}_P$ is the reaction rate based on the product, $\mathrm{MW}_{\mathrm{mix}}$ is the mixture molecular weight, ρ is the mixture mass density, A, b, E_a, m, and n are the pre-exponential factor, temperature exponent, activation energy, and reaction orders with respect to the fuel and oxygen, respectively, and R_u is the universal gas constant. In the present work, $A=5.1\times 10^{11}$ in cm mol s units, $b=0$ and $E_a=1\times 10^5$ J/mol, and $m=n=1$. These model choices are close to those employed in the DNS studies of Sreedhara and Laksmisha[34] in n-heptane diffusion flames evolving in isotropic turbulence under the pressures (=40 bars) and temperatures employed here. Moreover, the chosen values result in steady extinction limits (χ_e) comparable to detailed kinetic models for n-heptane[35] for the pressures and temperatures simulated here. Hence, the choice of a chemical time scale using the single-step model coupled with the vortex characteristics (length and velocity scales) allows us to construct the governing nondimensional numbers for the flame-vortex interaction, which are discussed in the next section. CHEMKIN subroutines are interfaced with the FLEDS code for the computation of kinetic source terms and transport properties. The simplified unity-Lewis number assumption is employed to model multicomponent species diffusion.

In Sec. III that follows, we will first discuss the important nondimensional numbers for the flame-vortex interactions derived from turbulent statistics in the near field of a high-Reynolds number jet, and then present results of the unsteady flame structure for a baseline case, and across a range of nondimensional parameters.

III. RESULTS AND DISCUSSION

Table I shows the important nondimensional numbers for the flame-vortex interaction studies, and their estimated range of values along with the expected physical effects. The length scales and velocity scales selected in this work are relevant to the near field of diesel jets where the jet Reynolds number is of the order of 100 000. Consider a diesel injection event from an orifice of diameter 150 μm, and injection velocity of 500 m/s. The equivalent constant-density gas jet has a diameter (d) of O(1 mm) and the same injection velocity.[36,37] If a spreading rate of 0.095 is assumed for the jet and the turbulent length scale is assumed to be 0.15 of the jet half-width,[38] the value of the length scale at 30d is about 430 μm. Length scales at shorter axial distances will be even smaller. The vortex length scales selected in this work lie in the range of 100–400 μm, which represent integral scales at axial locations upstream of 30d. If a centerline velocity decay constant of about 6.0 is assumed,[38] the jet centerline velocity at an axial distance of 30d will be about 100 m/s. The turbulence intensity will be a maximum of about 25 m/s at a normalized radial distance ($r/r_{1/2}$, where r

TABLE I. Nondimensional numbers for the flame-vortex interaction studies.

Numbers	Effect	Range simulated ($12 \leq x/d \leq 20$)
Length-scale ratio, $l_r = d_v/\delta$	Curvature	0.3–3.0
Velocity-scale ratio, $u_{fv} = u_v/u_f$	Unsteadiness	1.0–6.0
Damkőhler number, $\mathrm{Da} = \chi_{st}^{-1}/\tau_c$	Extinction, Da<1	Initial value (strength of the flame): 10–100
Reynolds number, $\mathrm{Re}_v = u_v^* d_v/\nu$	Unsteadiness, curvature, and viscous	60–2000 (prior works, $\mathrm{Re}_v < 600$)
Scalar dissipation ratio, $\chi_r = \chi_{st}/\chi_e$, $t^* = t/t_{eddy}$	Unsteadiness	Computed during the simulation

is the radial distance and $r_{1/2}$ is the jet half-width) of about 0.5. The flame is, however, located in the near-stoichiometric mixtures at radial distances greater than the jet half-width. At this radial distance, the turbulence intensity (q) will be lower. The values selected in our work lie in the range of 2–9 m/s, which are representative of turbulent velocity scales at the mean stoichiometric locations in the jet. Notice from Table I that in addition to the parameters defined in Fig. 1, the flame velocity scale $u_f(=\delta/\tau_c)$ and the eddy turnover time scale $t_{eddy}(=d_v/u_v)$ are employed to define nondimensional numbers for the velocity scale and time elapsed, respectively.

We observe from Table I that the simulated vortex-to-diffusion layer length scale ratios l_r lie in the range of 0.3–3.0. For a jet Reynolds number of the order of 100 000, the Taylor microscales (λ) are typically about ten times smaller than the integral length scales (L), while the Kolmogorov scales (η) are about two orders of magnitude smaller than L.[37] Since the largest vortex simulated here is of the order of L, the range of l_r (0.3–3.0) simulated correspond to vortices that are sized about three to ten times larger than λ, and about 30–100 times larger than η. Moreover, the simulated flames are much thicker (about two orders of magnitude larger) than the Kolmogorov scales. However, these scales would not significantly alter the flame structure due to overriding effects of viscous action. We will revisit viscous effects later in this paper.

Hence, the chosen range of length scales represents the inertial scales of the turbulent spectrum reasonably well. It is clear that l_r is a measure of the vortex-induced flame curvature. Similarly, the vortex-to-flame velocity scale ratios u_{fv} lie in the range of 1.0–6.0, and the relatively large values (>1.0) simulated indicate that unsteady effects on the flame response may be important. The lower limit of the vortex velocity roughly corresponds to the weakest vortex that can cause local extinction of the flames for the pressures and temperatures simulated here.

In the present work, the instantaneous flame-response is characterized by the flame Damkohler number Da, which is the ratio of the instantaneous flow time scale χ_{st}^{-1} and the instantaneous chemical time scale τ_c given by the single-step kinetic model [see Eq. (2)]. As discussed by Peters[9] and in our recent flame-vortex studies,[15] $\mathrm{Da} \leq 1$ may be used as a criterion for the onset of extinction, at which the χ_{st}^{-1} becomes just shorter than τ_c. The initial value of Da, Da_i, represents the strength of the initial flame, and its departure from extinction. The range of 10–100 simulated here represents moderately strained to highly strained flamelets that may occur in the near field of a high-Re jet.

We observe from Table I that the chosen vortex characteristics result in relatively large values of the Reynolds number, Re_v. The implications of high-Reynolds numbers are discussed in our recent publication,[15] and we will confirm some of the earlier findings in the present work as well. Note that apart from being a measure of the importance of viscous effects, Re_v represents the combined effects of unsteadiness and curvature since it involves both the vortex length and velocity scales. In addition to u_{fv}, we employ a scalar dissipation ratio χ_r, which is the ratio of the instantaneous stoichiometric scalar dissipation rate χ_{st} to the steady extinction limit χ_e, to quantify unsteady effects. As discussed in our recent works,[15,20] burning flames with values of χ_r greater than 1 indicate effects due to unsteadiness and departure from steady behavior. In the discussion of the results from the flame-vortex interaction studies, we will first investigate the transient flame response for a baseline case, and then explore effects due to unsteadiness and curvature on the vortex-induced flame dynamics.

To investigate the transient flame response, let us consider the case with $l_r = 1.5$, $u_{fv} = 5.85$, $\mathrm{Da}_i = 30$, and $\mathrm{Re}_v = 540$. Figures 2(a)–2(f) show the sequence of events that occur during the flame-vortex interaction in terms of temperature contours. We observe that the vortex impinges on the initially flat (one-dimensional) flame, and then induces strain and curvature as time progresses. Local extinction occurs by $t^* = 1.4$, when we observe relatively low temperatures (<1400 K) along the symmetry axis.

It is interesting to observe from Fig. 2(c) that the maximum value of χ_r along the symmetry axis is about 2, implying that the vortex-perturbed flame quenches at scalar dissipation rates values greater than χ_e. This reflects effects due to unsteadiness, which result in a delayed response of the flame and render the unsteady flame more resistant to extinction. Notice from Fig. 2(c) that edge flames, the dynamics of which would govern the subsequent evolution of the extinguished regions, surround the quenched regions. Accord-

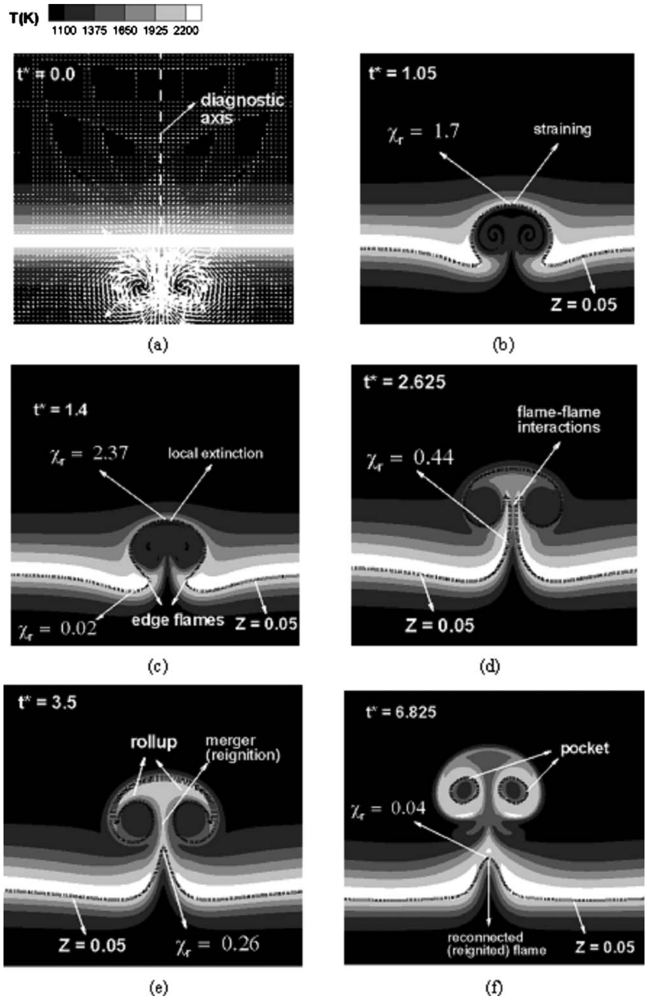

FIG. 2. Evolution of temperature (k) during the flame-vortex interaction for the baseline case [only one-third of vectors shown in (a) for clarity].

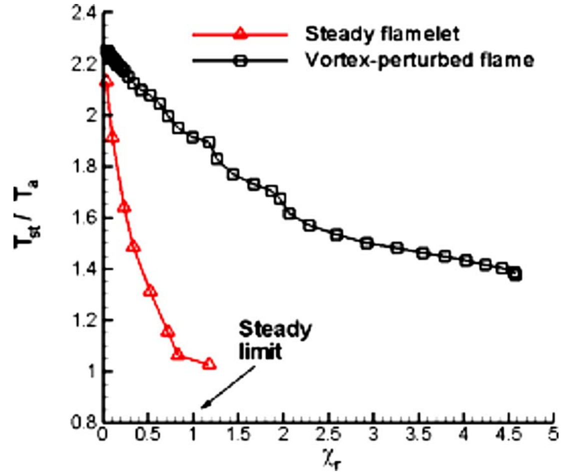

FIG. 3. (Color online) Normalized temperature T_{st}/T_a as a function of χ_r during the extinction phase of the flame-vortex interaction for the baseline case.

ingly, we observe from Figs. 2(d) and 2(e) that the edge flames are rolled up due to the vortex-induced recirculation. Through a series of transient events that involve mutual interactions (i.e., flame-flame interactions) between the edge flames and their merger, a reconnected (i.e., reignited) diffusion flame is established by about $t^*=6.8$, which is also surrounded by detached fuel-rich pocket. Hence, for the simulated conditions, the flame-vortex interaction outcomes are characterized by *unsteady extinction, reignition*, and *pocket formation*. In the subsequent analysis, we will choose the symmetry axis (i.e., the vertical centerline) as the diagnostic axis, and investigate the unsteady flame response. Note that this diagnostic axis represents a stretched flamelet that undergoes extinction and reignition due to the vortex-induced perturbation.

Figure 3 shows the unsteady flame temperature T_{st} at the stoichiometric mixture fraction normalized by the ambient temperature T_a. Also shown is the normalized temperature computed from a steady-flamelet model. We observe that the unsteady flame temperature is significantly higher than that predicted by the steady flamelet, indicating a delayed response of the vortex-perturbed flame. To estimate the unsteady extinction limit, consider Fig. 4, which shows the instantaneous Damkohler number (Da) as a function of the scalar dissipation ratio, χ_r. In addition to the baseline case ($u_{\mathrm{fv}}=5.85$), additional cases with $u_{\mathrm{fv}}=2.48$ and 1.24 are also shown. In Fig. 4, Da is computed as

$$\mathrm{Da}=\frac{[\dot{w}_c(Z,\chi,c)/\rho]}{\chi_{\mathrm{st}}}, \tag{3}$$

where $\dot{w}_c(Z,\chi,c)$ represents the source term of the reaction progress variable c. Here, c is computed as[39] $c=Y_{CO_2}+Y_{H_2O}$, and Eq. (2) is employed for the estimation of $\dot{w}_c(Z,\chi,c)$.

We observe from Fig. 4 that Da decreases as χ_r increases, and decreases below unity, which indicates the onset of local extinction when the mixing time scale becomes just shorter than the chemical time scale. Notice that when Da=1, the cases with $u_{\mathrm{fv}}=5.85$ and 1.24 have χ_r values of about 2.1 and 1.5, respectively, indicating that the unsteady flame quenches at values higher than the steady limit χ_e, and the unsteady limit decreases with decreasing vortex velocity scales. These trends agree well with the recent observations of Oh *et al.*[14] on vortex-induced extinction of methane-air

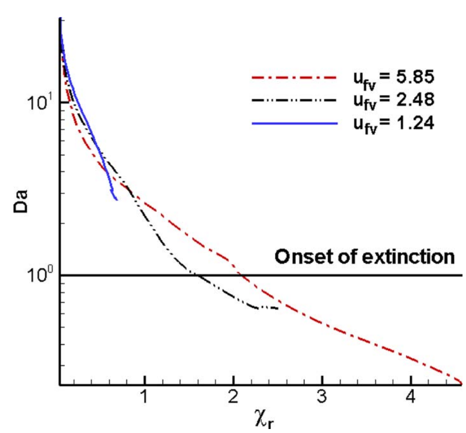

FIG. 4. (Color online) Da as a function of χ_r during the extinction phase for different values of u_{fv} for $l_r=1.5$ and $\mathrm{Da}_i=30$.

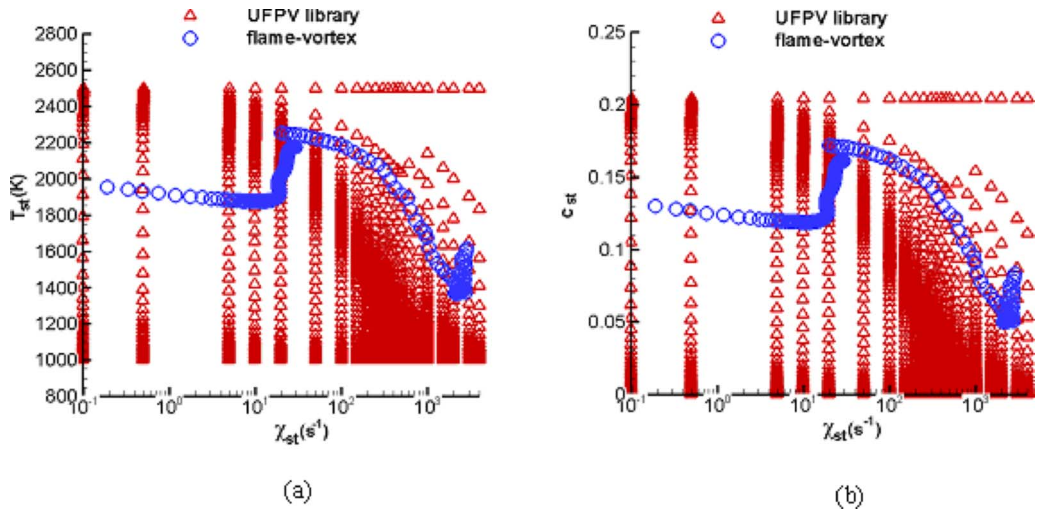

FIG. 5. (Color online) State points during the flame-vortex interaction and from a UFPV library for (a) T_{st} and (b) c_{st}.

flames. Moreover, the departure of the unsteady limit from χ_e and its flow dependence confirm that the extinction criterion, $\chi=\chi_e$ is inappropriate for unsteady flames. As discussed by Katta *et al.*,[13] an extinction criterion solely based on the scalar dissipation rate is not applicable for unsteady flames, since χ is the dissipation rate of a passive scalar, and hence does not account for chemical phase-lag effects. In this context, the present extinction criterion of $\mathrm{Da}\leq 1$ is more meaningful, as the progress variable source term [see Eq. (3)] accounts for chemical lag. Furthermore, this criterion is amenable to implementation in large-scale RANS/LES of jet flames, as $\dot{w}_c(Z,\chi,c)$ can be determined as the conditional-mean source term of the mean/filtered progress variable[39] which would appear as a tracking scalar in addition to the mean/filtered mixture fraction.

With respect to reignition following extinction, the physical mechanisms governing the scenarios observed in Figs. 2(c)–2(f) were clarified in our recent studies of flame-vortex interactions under typical diesel conditions,[15,20] as discussed in Sec. I. With respect to 3D effects, such as vortex stretching, it is expected that the extinction phase would be minimally affected as curvature effects are not important, whereas the reignition phase would be affected due to species and heat diffusion in both lateral (x) and transverse (z) directions. In other words, while the physical mechanisms for reignition involving edge-flame dynamics and curvature effects would remain unaffected in a 3D flow field, the magnitudes of time scales and scalar dissipation rates may differ from those in a 2D flow field.

In the context of modeling, we need to account for the influence of the neighboring edge flames on the quenched regions to predict the reignition scenarios observed here. In the following, we discuss a flamelet-based modeling approach that employs the reaction progress variable c (Refs. 9 and 39) in addition to the scalar dissipation rate χ to account for edge-flame effects. Consider Figs. 5(a) and 5(b) which show the state points during extinction and reignition in T_{st}-χ_{st} and c_{st}-χ_{st} spaces, respectively, along the symmetry axis. Also shown in the figures are states obtained from a UFPV library. The variable c_{st} is computed as the sum of major product mass fractions, i.e., $c=Y_{CO_2}+Y_{H_2O}$, at the stoichiometric mixture fraction.

It is interesting to observe from Fig. 5(a) that there exist vortex-perturbed flame states with the same value of χ_{st}, but different values of T_{st} and c_{st} and vice versa. These different states represent different temporal stages during unsteady extinction/reignition. Such transient states cannot be recovered using steady flamelet[9] [i.e., $T=\mathrm{fn}\ (Z,\chi)$] and steady flamelet/progress variable[39] (FPV) [i.e., $T=\mathrm{fn}\ (Z,c)$] models that assume T to be single-valued functions of χ and c, respectively, for a given Z. Hence, a complete description of the unsteady flame states observed in the flame-vortex simulation can be achieved by employing both χ_{st} and c_{st} as parameters. Pitsch and Ihme[40] recently employed such a parametrization in an *unsteady* FPV (UFPV) model to simulate a coaxial swirled gas turbine combustor using LES. In the context of the unsteady flames investigated here, the parametrization used in the UFPV model, $T=\mathrm{fn}\ (Z,\chi,c)$, employs χ to represent the flow-unsteadiness, while the chemical-unsteadiness is contained in c. Note that prior works so far have not assessed the fidelity of the UFPV approach to predict unsteady extinction/reignition, which is demonstrated below.

In addition to the flame-vortex simulation results, Figs. 5(a) and 5(b) show state points computed using the unsteady flamelet equations.[9] These state points are obtained from stand-alone flamelet computations (i.e., independent of the flame-vortex simulations) corresponding to a wide range of χ_{st} values $(2\mathrm{e}-4\chi_e\leq\chi_{st}\leq 8\chi_e)$. These transient states are bounded by the equilibrium burning and frozen solutions. Note that we have employed 23 values of χ_{st} and $100(c,T,Y_i)_{st}$ states for each value of χ_{st} to generate the library. We observe from the figures that the flame-vortex states lie within the library, and are fairly close to the state points in the library. Furthermore, since the UFPV library is generated using the *unsteady* flamelet equations, it accounts for the transient partially burned states that are encountered during the transition from unburned to burned states and vice versa for each value of χ. On the other hand, a steady FPV

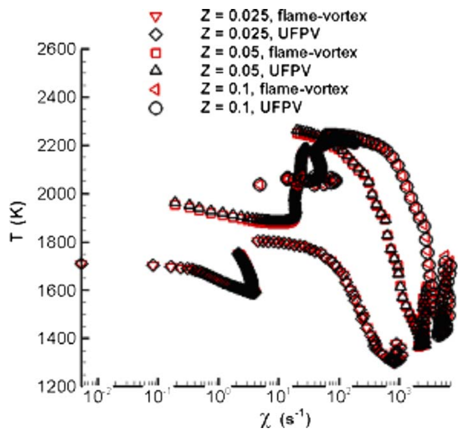

FIG. 6. (Color online) Comparison of flame-vortex results and UFPV model predictions, baseline case.

model[39] accounts only for the states along the middle branch of the steady-state S curve[9] in addition to the lower (unburned) and upper (burned) branches, and hence does not capture the transient states that are observed in Figs. 5(a) and 5(b) from the flame-vortex simulation results.

Figure 6 compares the predicted values of the temperature T using the UFPV model with the flame-vortex simulation results for three mixture fractions, $Z=0.05$ (stoichiometric), $Z=0.025$ (lean), and $Z=0.1$ (rich). To obtain the results shown in Fig. 6, libraries similar those shown in Figs. 5(a) and 5(b) were generated for the lean and rich fractions. For a given value of Z, the UFPV model results are obtained through 2D interpolation based on χ and c estimated from the flame-vortex simulation along the vertical centerline as a function of time. UFPV model predictions and the flame-vortex results for all the three values of Z agree within 3%. This validates the primary assumption of the UFPV approach that the unsteady flame is completely specified by the instantaneous scalar dissipation rate χ and the instantaneous progress variable c for a given value of Z. It is important to note that the UFPV library represents unsteady nonpremixed flamelets, whereas the vortex-induced curvature creates locally premixed regions in the vortex-perturbed flame. Essentially, local premixing effects due to heat and species diffusion from the edge flames manifest as changes in c. These changes, in turn, manifest as different transient nonequilibrium states in the UFPV library. Hence, our work shows that unsteady nonpremixed flamelets parametrized by Z, χ, and c (i.e., UFPV libraries) are applicable for the prediction of transient partially premixed flames (such as the present vortex-perturbed flames). Vreman *et al.*[41] arrived at a similar conclusion from their LES-based modeling studies of Sandia flames D and F using both premixed and nonpremixed flamelet manifolds. The authors found that predictions from premixed and nonpremixed flamelets showed minor differences with respect to flame temperature and major species, implying that nonpremixed flamelets with the appropriate parametrization are applicable for the simulation of partially premixed flames. Note, however, that Vreman *et al.*[41] employed a steady-flamelet parametrization, i.e., $T=\text{fn}\ (Z,c)$, similar to the FPV model of Pierce and Moin.[39] As discussed before, such a parametrization is not unique and cannot distinguish between transient burning and partially burning (i.e., reignited) states, and hence is not applicable for the highly unsteady flamelets considered here.

Agreement similar to that shown in Fig. 6 was obtained with respect to species mass fractions as well. In the case of detailed chemistry, the UFPV library could be relatively large. However, once the library is generated, the computational costs involved are primarily due to interpolation, which would be much lower than those due to direct integration with detailed chemistry. Hence, the present work shows that the UFPV model can adequately describe unsteady flame extinction and reignition scenarios, provided the instantaneous scalar dissipation rate $\chi(Z,t)$ and the progress variable $c(Z,\chi,t)$ are accurately specified as model parameters. However, in the context of employing the UFPV formulation as a RANS/LES submodel, modeling of the conditional source term $\dot{w}_c(Z,\chi,c)$ of the progress variable c would be required. As discussed before, one approach is to directly tabulate $\dot{w}_c(Z,\chi,c)$ from the flamelet equations.[39] Such an approach can account for reignition through autoignition, but not through edge-flame interactions that involve curvature (i.e., lateral diffusion) effects. To account for reignition through edge-flame dynamics, the progress variable source term would have to be related to edge-flame characteristics, such as the edge displacement speed.[10]

From a modeling perspective, it is useful to understand how unsteadiness and curvature affect the flame-vortex dynamics and the validity of flamelet models. In the context of the jet near field, variation in unsteady and curvature effects may occur as we progress axially downstream in the jet. In particular, while the turbulent length scales would increase in a linear fashion,[37,42] the scalar dissipation rates would show more drastic (x^{-4}) decay as we proceed downstream in the jet,[37,43] leading to relatively thicker diffusion layers. This implies that the vortex-to-diffusion length scale ratios (l_r) would decrease with increasing axial locations in the jet. Similarly, decreasing turbulent velocity scales would result in lower values of vortex-to-flame velocity scale ratios (u_{fv}) at downstream jet locations. We explore these scenarios in the analysis below through comparisons of the baseline case considered so far ($l_r=1.5$, $u_{\text{fv}}=5.85$, $\text{Da}_i=30$) with cases represented by the following nondimensional numbers, $l_r=0.98$, $u_{\text{fv}}=3.86$, $\text{Da}_i=40$ and $l_r=0.67$, $u_{\text{fv}}=2.27$, $\text{Da}_i=60$, which denote flame-vortex interactions at downstream jet locations involving relatively slower vortices interacting with relatively thicker flames.

Figure 7 shows Da and χ_r as a function of t^* during the extinction phase of the flame-vortex interactions for different values of Da_i. We observe that as Da_i increases, the extinction time scales are longer, implying that the flames are more resistant to extinction. This is consistent with in the interpretation of Da_i as a flame-strength parameter. In addition, Fig. 7 shows that the peak magnitude and rate of increase in χ_r decrease with increasing Da_i, which is consistent with the trends associated with the decrease in u_{fv} (relatively slower vortices) discussed in our recent flame-vortex interaction studies.[15] Essentially, faster vortices result in higher magnitudes and rates of increase of χ_r. Furthermore, invoking the

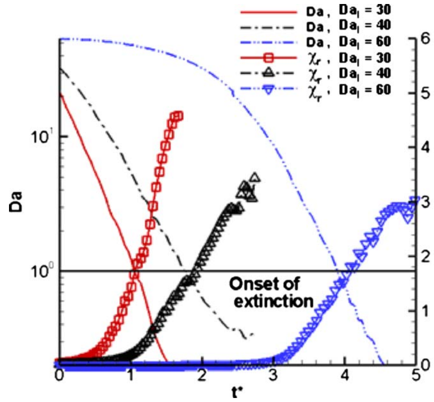

FIG. 7. (Color online) Da and χ_r as a function of t^* during the extinction phase for conditions corresponding to different axial locations in the jet.

unsteady extinction criterion of $\mathrm{Da} \leq 1$ discussed before, it may be seen from Fig. 7 that the unsteady extinction limit (at $\mathrm{Da}=1$) moderately decreases (by about 18%) as Da_i increases from 30 to 60. Hence, it is expected that as we proceed downstream in the jet near field, lower values of u_{fv} and higher values of Da_i would be encountered, which would diminish unsteady effects on local flame extinction, and steady extinction limits would be applicable. Let us now compare the flame response during the reignition phase for conditions relevant to downstream jet locations.

The time evolution of the instantaneous flame Damköhler number Da during extinction/reignition of the vortex-perturbed flames for the range of Da_i considered is shown in Fig. 8. We observe strong overshoots in Da following extinction in all cases, which marks the onset of reignition under the influence of edge flames bordering the extinguished regions. The presence of significant amounts of diluted fractions in the extinguished regions leads to relatively low mixing rates, and hence relatively large values of Da. With subsequent partial premixing promoted by heat and species diffusion from the adjoining edge flames, Da gradually relaxes to values comparable to the original diffusion flame, as the reigniting flamelets evolve into a reconnected diffusion flame.

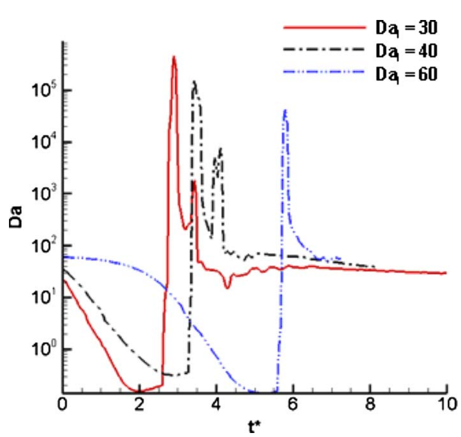

FIG. 8. (Color online) Da as a function of t^* along the vertical centerline during the flame-vortex interactions corresponding to different values of Da_i.

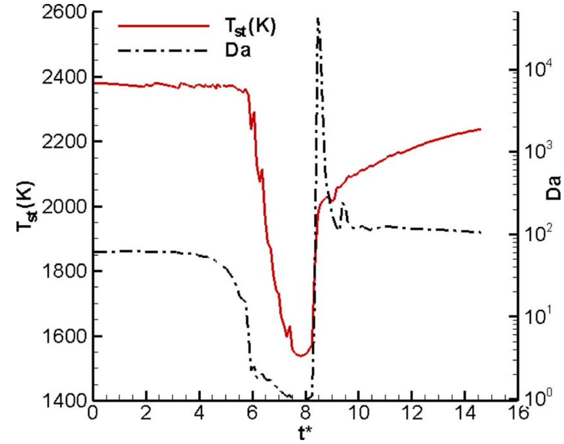

FIG. 9. (Color online) $T_{\mathrm{st}}(k)$ and Da as a function of t^* along the vertical centerline during the flame-vortex interactions with the set of parameters given by $l_r=0.335$, $u_{\mathrm{fv}}=2.27$, $\mathrm{Da}_i=60$.

We observe from Fig. 8 that even though the time scales for extinction increase from $\mathrm{Da}_i=30$ to $\mathrm{Da}_i=60$, as discussed before, the time scales for reignition show the opposite trend. In particular, it is estimated from Fig. 8 that the reignition phase occurs over nondimensional times $t^*=7.4$, 4.9 and 1.7 corresponding to $\mathrm{Da}_i=30$, 40, and 60, respectively. In terms of physical time, this represents about a 60% decrease in reignition time scale from $\mathrm{Da}_i=30$ to $\mathrm{Da}_i=60$. On the other hand, it is estimated that the extinction time scale roughly increases by about 24% from $\mathrm{Da}_i=30$ to $\mathrm{Da}_i=60$. This indicates the dominating influence of decreasing l_r values at downstream jet locations, which result in increasing flame curvature and faster reignition under the influence of edge flames surrounding the quenched regions.[15,20] For instance, the 60% decrease in the reignition time scale roughly correlates with the 55% decrease in the length scale ratio l_r from 1.5 at $\mathrm{Da}_i=30$ to 0.67 at $\mathrm{Da}_i=60$. Hence, as we proceed downstream axially in the near field of a high-Re jet, it is expected that *decreasing unsteady effects lead to longer flame extinction time scales*, while *increasing curvature effects contribute toward shorter reignition time scales*. In other words, at downstream jet locations, it is harder to extinguish the flame, and if the flame is extinguished, it is easier to reignite it. These factors can contribute to the quasisteady lift-off height in a reacting jet.

From a modeling viewpoint, it is useful to investigate the effects due to relatively small scales on the local flame structure. For instance, consider flame-vortex interactions for the set of nondimensional numbers given by: $l_r=0.335$, $u_{\mathrm{fv}}=2.27$, $\mathrm{Da}_i=60$. Here, $l_r=0.335$ corresponds to an eddy that is sized about 20% of the integral length scale L and roughly 20 times the Kolmogorov scale η in the near field of a high-Re ($\sim$100 000) jet.[37] Since we are exploring conditions relevant to the jet near-field region, the vortex is relatively strong ($u_{\mathrm{fv}}>2$), and interacts with a relatively strong flame ($\mathrm{Da}_i=60$).

Figure 9 shows the temperature T_{st} and the flame Damkőhler number Da at the stoichiometric mixture fraction along the vertical centerline as a function of t^* during the flame-vortex interaction. We observe that the flame tempo-

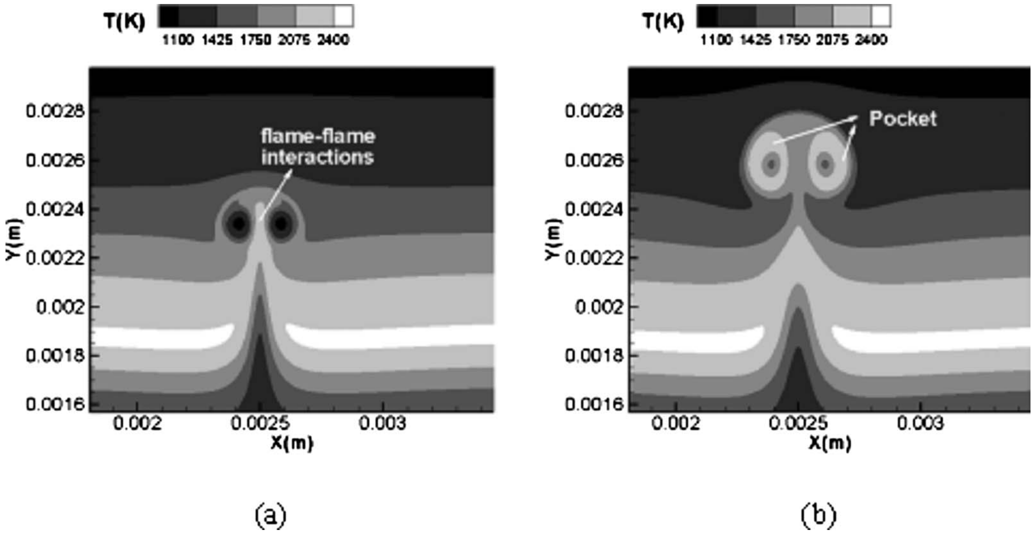

FIG. 10. Contours of temperature (k) during interaction during the interaction of a relatively small vortex () with the flame at (a) $t^*=9.1$, and (b) $t^*=14.6$.

rarily weakens and approaches extinction ($\mathrm{Da}\sim 1$) due to the vortex-induced strain, but rapidly reignites/recovers within one eddy turnover time ($t^*=1$). This indicates the strengthening effect due to flame-flame interactions resulting from the vortex-induced curvature.

Figures 10(a) and 10(b) show the instantaneous snapshots of temperature in the vortex-perturbed flame at $t^*=9.1$ and 14.6, respectively. We observe the effects due to flame-flame interactions leading to rapid flame recovery following flame weakening in Fig. 10(a), and Fig. 10(b) shows that by $t^*=14.6$, the diffusion flame has reconnected, and a detached fuel-side pocket has formed. Note that for even slower (or weaker) vortices, local extinction may be prevented due to curvature-induced flame-flame interactions, resulting in thickened diffusion flames surrounded by pockets. Hence, the present results indicate that at downstream jet locations and/or radial locations far from the jet centerline, we are likely to encounter regimes characterized by *pocket formation without extinction* due to the presence of relatively smaller ($l_r<0.3$) and relatively slower ($u_{\mathrm{fv}}<2$) vortices. Experiments of Thevenin *et al.*[44] in vortex-perturbed hydrogen flames have shown evidence of such regimes for relatively small vortex-to-flame length scale ratios ($0.1<l_r<1.0$). Furthermore, as discussed by Thevenin *et al.*,[44] below a certain vortex size ($l_r<0.1$), the effect of the vortex on the flame structure would be mitigated by viscous effects.

It is useful to summarize the interaction regimes observed in the flame-vortex interaction studies in an outcome diagram relevant for localized flame dynamics in the near field of high-Reynolds number jets. Figure 11 shows the outcome diagram constructed in terms of l_r and u_{fv} as axes, consistent with prior numerical[45] and experimental[44] works. In Fig. 11, Da_v is the vortex Damkőhler number, defined as

$$\mathrm{Da}_v = \frac{\tau_v}{\tau_c} = \frac{d_v}{u_v \tau_c}, \quad (4)$$

where τ_v denotes the characteristic chemical time scale of the vortex. Note that Da_v may be expressed in terms of l_r and u_{fv} as[15,45]

$$\mathrm{Da}_v = \frac{d_v}{u_v \tau_c} = \frac{l_r \delta}{u_v \tau_c} = \frac{l_r}{u_{\mathrm{fv}}}, \quad (5)$$

where $u_f=\delta/\tau_c$ is the velocity scale of the flame. In Fig. 11, U and C denote the magnitudes of effects due to unsteadiness and curvature. Moreover, the arrows indicate directions of increasing effects/magnitudes due to the controlling parameter (i.e., l_r or u_{fv}). As discussed in the results so far, unsteady effects diminish with decreasing velocity scale ratios and increasing flame Damkohler numbers, whereas curvature effects are enhanced with decreasing length scale ratios. As indicated in Fig. 11, these variations (i.e., decreasing unsteady effects and increasing curvature effects) are likely to occur as we proceed axially downstream in the near field of a high-Re jet. Note that the outcome diagram shown in Fig. 11 does not show the exact limits of l_r and u_{fv} that demarcate different regimes, such as pocket formation, extinction/reignition and rollup and straining. Larger number

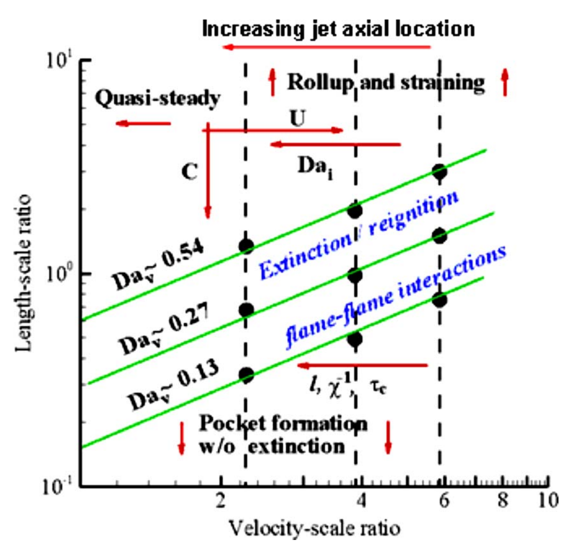

FIG. 11. (Color online) Outcome diagram based on flame-vortex interaction studies relevant to the near-field of high-Reynolds number jets.

of simulations over a wider range of conditions would be required to derive exact limits delineating different interaction regimes.

In Fig. 11, each of the constant Da_v lines represents compensatory changes in the vortex time scale τ_v and the chemical time scale τ_c, or l_r and u_{fv} in nondimensional terms [see Eqs. (4) and (5)]. In the context of the jet near field, progressing from right to left along a constant Da_v line is similar to progressing axially downstream in the jet, which leads to decreasing l_r and u_{fv} values, and increasing Da_i values. As discussed before, decreasing l_r values have a dominating effect on reignition dynamics, resulting in faster reignition, while decreasing u_{fv} values predominantly affect extinction by leading to longer extinction time scales. In addition, Fig. 11 shows that with relatively small l_r and u_{fv} values, more likely at downstream jet locations, we would encounter pocket formation regimes without local extinction. Moreover, for relatively large values of $l_r(\geq 3.0)$, we recover the more familiar regimes of flame rollup and straining, which have been reported in prior flame-vortex interaction studies.[44,45] It is important to note that the flame-vortex interaction regimes shown by the outcome diagram depend only on the nondimensional numbers, such as l_r and u_{fv}, and hence valid for a wide range of vortex and flame characteristics that result in similar values of these numbers.

Note, however, that the outcome diagram shown in Fig. 11, and the conclusions drawn in this work are based on *single*-vortex-flame simulations, whereas in reality, the flamelet in a turbulent flow field would interact with a spectrum of vortices. The present work provides useful insights into the detailed effects of isolated vortices on the local flame extinction/reignition and the validity of modeling approaches. It is evident, however, that by considering an isolated vortex-perturbed flame, we cannot gain insight into the relative probabilities of local extinction/reignition events in a large-scale jet flame, and the extent to which these events may affect outcomes, such as flame lift-off height.

IV. SUMMARY AND CONCLUSIONS

In the present work, we investigated the dynamics of flame-vortex interactions relevant to the near-field of high-Reynolds number jets. The pressure and temperature simulated were representative of conditions in practical combustors such as diesel engines. A single-step kinetic model for *n*-heptane oxidation was employed.

The flame-vortex interactions were characterized by the following nondimensional numbers: vortex-to-flame length scale ratio (l_r), the vortex-to-flame velocity scale ratio (u_{fv}), the flame Damkőhler number (Da), and the vortex Reynolds number (Re_v). The range of numbers represented relatively small vortices ($l_r < 3.0$), relatively fast vortices ($u_{fv} > 1.0$), and relatively strong flames ($Da_i > 10$). Results showed that the unsteady flame response is characterized by local extinction followed by reignition and pocket formation. Due to unsteady effects that result in a delayed response of the flame, unsteady extinction limits up to two times the steady values were observed. An extinction criterion based on the instantaneous flame Damkőhler number (i.e., Da=1) applicable for unsteady flames was discussed. The extension of this criterion to RANS/LES of large-scale jet flames, in terms of the conditional-mean scalar dissipation rate and the conditional source term of a reactive scalar (progress variable) was explored. In addition, a UFPV model with the instantaneous scalar dissipation rate and the instantaneous progress variable as model parameters were shown to accurately describe the unsteady extinction/reignition scenarios observed in the flame-vortex studies.

In order to understand how the nature of local flame dynamics changes with increasing axial locations in a jet, effects due to decreasing length scale ratios (l_r), decreasing velocity scale ratios (u_{fv}), and increasing flame Damkohler numbers (Da_i) on flame extinction/reignition were explored. Results showed diminishing unsteady effects due to decreasing values of u_{fv}, and increasing curvature effects due to decreasing values of l_r. Accordingly, while extinction time scales were found to increase with lower l_r and u_{fv} values, reignition time scales were found to decrease. Consequently, for relatively smaller length scales ($l_r \sim 0.3$), reignition through flame-flame interactions were strong enough to prevent local extinction, resulting in pocket-formation-without-extinction regimes. The observed flame-vortex interaction outcomes, and trends in unsteady and curvature effects, were summarized on an outcome diagram with l_r and u_{fv} as axes, which is relevant for near-field jet flame dynamics.

Hence, the present work underscores the importance of unsteady extinction/reignition events in the near-field of high-Re jets, such as those occurring in diesel engine applications. In the context of turbulent combustion modeling, this work demonstrates the need for improved modeling approaches, such as unsteady flamelet/progress variable models, which can account for both unsteady and curvature effects during extinction/reignition. These findings notwithstanding, the implications of some of the key assumptions, such as single-vortex-flame simulations need further assessment.

ACKNOWLEDGMENTS

The numerical code employed in this work was developed by Professor Vinicio Magi. The authors thank him for useful discussions during the course of this study. Computing resources for this work were provided by the National Center for Supercomputing Applications (NCSA) through Grant No. MCAO6N038 and the Rosen Center for Advanced Computing at Purdue University.

[1]D. L. Siebers, B. S. Higgins and L. M. Pickett, "Flame lift-off on direct-injection diesel fuel jets: Oxygen concentration effects," SAE Paper No. 2002-01-0890 (Society of Automotive Engineers, Warrendale, PA, 2002).
[2]L. M. Pickett and D. L. Siebers, "Soot in diesel fuel jets: effects of ambient temperature, ambient density, and injection pressure," Combust. Flame **138**, 114 (2004).
[3]R. Venugopal and J. Abraham, "A review of fundamental studies relevant to flame lift-off in diesel jets," SAE Paper No. 2007-01-0134 (Society of Automotive Engineers, Warrendale, PA, 2007); also appears in SAE Trans. J. Eng. **116**, 132 (2007).
[4]R. Venugopal and J. Abraham, "A numerical investigation of flame lift-off in diesel jets," Combust. Sci. Technol. **179**, 2599 (2007).
[5]P. K. Senecal, E. Pomraning, and K. J. Richards, "Multidimensional modeling of direct-injection diesel spray liquid length and flame lift-off length

using CFD and parallel detailed chemistry," SAE Paper No. 2003-01-1043 (Society of Automotive Engineers, Warrendale, PA, 2003).
[6]R. R. Cao, S. B. Pope, and A. R. Masri, "Turbulent lifted flames in a vitiated coflow investigated using joint PDF calculations," Combust. Flame **142**, 438 (2005).
[7]S. K. Aggarwal, "A review of spray ignition phenomena: present status and future research," Prog. Energy Combust. Sci. **24**, 565 (1998).
[8]L. Vervisch and T. Poinsot, "Direct numerical simulation of non-premixed turbulent flames," Annu. Rev. Fluid Mech. **30**, 655 (1998).
[9]N. Peters, *Turbulent Combustion* (Cambridge University Press, Cambridge, UK, 2000), pp. 229–235.
[10]H. G. Im and J. H. Chen, "Structure and propagation of triple flames in partially-premixed hydrogen-air mixtures," Combust. Flame **119**, 436 (1999).
[11]N. Peters and F. A. Williams, "Lift-off characteristics of turbulent jet diffusion flames," AIAA J. **21**, 423 (1983).
[12]V. S. Santoro, D. C. Kyritsis, A. Linan, and A. Gomez, "Vortex-induced extinction behavior in methanol gaseous flames: A comparison with quasi-steady extinction," Proc. Combust. Inst. **28**, 2109 (2000).
[13]V. R. Katta, T. R. Meyer, M. S. Brown, J. R. Gord, and W. M. Roquemore, "Extinction criterion for unsteady, opposing-jet diffusion flames," Combust. Flame **137**, 198 (2004).
[14]C. B. Oh, C. E. Lee, and J. Park, "Numerical investigation of extinction in a counterflow non-premixed flame perturbed by a vortex," Combust. Flame **138**, 225 (2004).
[15]R. Venugopal and J. Abraham, "A 2-D DNS investigation of extinction and reignition dynamics in non-premixed flame-vortex interactions," Combust. Flame **153**, 442 (2008).
[16]V. S. Santoro, A. Linan, and A. Gomez, "Propagation of edge flames in counterflow mixing layers: experiments and theory," Proc. Combust. Inst. **28**, 2039 (2000).
[17]V. S. Santoro and A. Gomez, "Extinction and reignition in counterflow spray diffusion flames interacting with laminar vortices," Proc. Combust. Inst. **29**, 585 (2002).
[18]P. Sripakagorn, S. Mitarai, G. Kosaly, and H. Pitsch, "Extinction and reignition in a diffusion flame: A direct numerical simulation study," J. Fluid Mech. **518**, 231 (2004).
[19]M. Hermanns, M. Vega, and A. Linan, "On the dynamics of flame-edges in diffusion-flame/vortex interactions," Combust. Flame **149**, 32 (2007).
[20]R. Venugopal and J. Abraham, "Numerical investigations of reignition in vortex-perturbed n-heptane non-premixed flames," AIAA J. **46**, 2479 (2008).
[21]J. D. Buckmaster, "Edge flames," Prog. Energy Combust. Sci. **28**, 435 (2002).
[22]G. Amantini, J. H. Frank, and A. Gomez, "Experiments on standing and traveling edge flames around flame holes," Proc. Combust. Inst. **30**, 313 (2005).
[23]G. Amantini, J. H. Frank, B. A. V. Bennett, M. D. Smooke, and A. Gomez, "Comprehensive study of the evolution of an annular edge flame during extinction and reignition of a counterflow diffusion flame perturbed by vortices," Combust. Flame **150**, 292 (2007).
[24]J. Abraham and V. Magi, "Exploring velocity and density ratio effects in a mixing layer using DNS," Int. J. Comput. Fluid Dyn. **8**, 147 (1997).
[25]A. Viggiano and V. Magi, "A 2-D investigation of n-heptane autoignition by means of direct numerical simulation," Combust. Flame **137**, 432 (2004).
[26]J. W. Anders, V. Magi, and J. Abraham, "Large-eddy simulation in the near field of a transient multicomponent gas jet with density gradients," Comput. Fluids **36**, 1609 (2007).
[27]S. K. Lele, "Finite difference schemes with spectral-like resolution," J. Comput. Phys. **103**, 16 (1992).
[28]B. Carnahan, *Applied Numerical Methods* (Wiley, New York, 1969), p. 363.
[29]T. J. Poinsot and S. K. Lele, "Boundary conditions for direct simulations of compressible viscous flows," J. Comput. Phys. **101**, 104 (1992).
[30]S. Liu, J. C. Hewson, J. H. Chen, and H. Pitsch, "Effects of strain rate on high-pressure non-premixed n-heptane autoignition in counterflow," Combust. Flame **137**, 320 (2004).
[31]A. R. Karagozian and F. E. Marble, "Study of a diffusion flame in a stretched vortex," Combust. Sci. Technol. **45**, 65 (1986).
[32]P. H. Renard, J. C. Rolon, D. Thevenin, and S. Candel, "Dynamics of flame/vortex interactions," Prog. Energy Combust. Sci. **26**, 225 (2000).
[33]C. Safta, S. Enachescu, and C. K. Madnia, "Interaction of a vortex ring with a diffusion flame," Phys. Fluids **14**, 668 (2002).
[34]S. Sreedhara and K. N. Lakshmisha, "Direct numerical simulation of autoignition in a non-premixed turbulent medium," Proc. Combust. Inst. **28**, 25 (2002).
[35]R. Seiser, H. Pitsch, K. Seshadri, W. J. Pitz, and H. J. Curran, "Extinction and autoignition of n-heptane in counterflow configuration," Proc. Combust. Inst. **28**, 2029 (2000).
[36]V. Iyer and J. Abraham, "Penetration and dispersion of transient gas jets and sprays," Combust. Sci. Technol. **130**, 315 (1997).
[37]R. Venugopal, "Numerical simulations of flame dynamics in the near-field of high-Reynolds number jets," Ph.D. thesis, Purdue University, 2008.
[38]S. B. Pope, *Turbulent Flows* (Cambridge University Press, Cambridge, UK, 2000), pp. 101 and 108.
[39]C. D. Pierce and P. Moin, "Progress-variable approach for large-eddy simulation of non-premixed turbulent combustion," J. Fluid Mech. **504**, 73 (2004).
[40]H. Pitsch and M. Ihme, "An unsteady flamelet/progress variable method for LES of non-premixed turbulent combustion," AIAA Paper No. 2005-0557 (American Institute of Aeronautics and Astronautics, Reston, VA, 2005).
[41]A. W. Vreman, B. A. Albrecht, J. A. van Oijen, L. P. H. de Goey, and R. J. M. Bastiaans, "Premixed and nonpremixed generated manifolds in large-eddy simulation of Sandia flame D and F," Combust. Flame **153**, 394 (2008).
[42]I. Wygnanski and H. Fiedler, "Some measurements in the self-preserving jet," J. Fluid Mech. **38**, 577 (1969).
[43]M. Namazian, R. W. Schefer, and J. Kelly, "Scalar dissipation measurements in the developing region of a jet," Combust. Flame **74**, 147 (1988).
[44]D. Thevenin, D. P. H. Renard, C. J. Fiechetner, J. R. Gord, and J. C. Rolon, "Regimes of non-premixed flame-vortex interactions," Proc. Combust. Inst. **28**, 719 (2000).
[45]B. Cuenot and T. Poinsot, "Effects of curvature and unsteadiness on diffusion flames: implications for turbulent diffusion combustion," Sym. (Int.) Combust., [Proc.] **25**, 1383 (1994).